Performance Analysis of MEMS-based Inertial Measurement Units in terrestrial vehicles

Domenico Capriglione[1], Marco Carratù[2], Marcantonio Catelani[3], Lorenzo Ciani[3], Gabriele Patrizi[3], Antonio Pietrosanto[2], Roberto Singuaroli[3], Paolo Sommella[2]

[1] *Department of Information and Electrical Engineering "Maurizio Scarano", University of Cassino and Southern Lazio, Via G. Di Biasio, 43, Cassino (FR), Italy, capriglione@unicas.it*
[2] *Department of Industrial Engineering, University of Salerno, Via Giovanni Paolo II, 132, Fisciano (SA), Italy, {mcarratu, apietrosanto, psommella}@unisa.it*
[3] *Department of Information Engineering, University of Florence, Via di S. Marta, 3, 50139, Florence, Italy, {marcantonio.catelani, lorenzo.ciani, gabriele.patrizi, roberto.singuaroli}@unifi.it*

***Abstract* — In the recent period, Inertial Measurement Units (IMUs) are widely employed in many applications, such as smartphones, robotics, Unmanned Aerial vehicles, automotive and self-driving vehicles, artificial intelligence, and numerous others. However, the dynamical metrological performances and the reliability analysis when these microelectronic devices operate under real environmental conditions are not sufficiently covered by scientific literature. Starting from standard tests for automotive applications, to emulate the real operating conditions of IMUs, a new test plan based on sine sweep vibration profiles has also been developed, including different service conditions characterized by the presence of a sinusoidal component with the addition of a random vibration noise typical of automotive scenarios. In-depth analysis has been carried out in the time and frequency domains leading to the employment of suitable figures of merit, highlighting the effects of mechanical stress on the metrological performances of microelectromechanical sensors. The developed test plan could be used to investigate if sinusoidal vibrations at specific frequencies influence the correct operation of low-cost platforms in typical automotive applications. The experimental results have confirmed the suitability of the proposed figures of merit in analyzing the effects of vibrations typical of the automotive context on the IMUs operating. In particular, they have allowed investigating the axes cross-sensitivity of triaxial systems, spurious responses, and unexpected behaviors due to the devices' non-ideality.**

***Keywords— Testing, Reliability, Accelerometer, Gyroscope, Metrological Performance, Automotive*.**

I. INTRODUCTION

Diagnostic and fault diagnosis are fundamental tools in several industrial fields since they let designers achieve high reliability and availability targets [1]-[3]. A condition monitoring (CM) system is one of the best solutions to achieve effective and efficient diagnostic. Several benefits could be obtained by means of CM, as follow: the need for corrective maintenance is minimized, artificial intelligence tools could be implemented to estimate the health-state of the system, the overall management costs are reduced, reliability and remaining useful life of the system could be easily evaluated [4]-[9].
Analytics based on large data sets have recently emerged in the industrial world; such analytics optimize production quality, save energy, optimize diagnostics and improve equipment service. In the Industry 4.0 context, the collection and comprehensive evaluation of data from many different sources (such as CM tools) will become standard support in real-time decision-making [10],[11].
In automotive applications, which is the topic of this work, Inertial Measurement Units (IMUs) are widely used, both as design requirements and diagnostic tools [12]-[16]. Consequently, the accuracy and reliability of IMUs become a fundamental topic to ensure the proper expected performance of this system and to guarantee its correct operating throughout the system life cycle.
Commercial IMUs typically integrate the following sensors (or a subset of these sensors):

- A triaxial accelerometer used to measure the linear acceleration toward the three axes;
- A triaxial gyroscope to acquire information on the angular rate of the system toward the three axes;

Several technologies of IMU are available in the market. To ensure small dimensions, low power dissipation, low-cost, high accuracy, and high stability, it is possible to use MEMS (Micro Electro Mechanical Systems) technology. Consequently, nowadays, MEMS-based IMUs are dominating the inertial platform market in every field of application. [17]-[20].
Recent literature extensively focuses on MEMS-based IMUs design and calibration (see, for instance, but not only [21]-[26]). Quite the opposite, the characterization of IMUs under a real operating context well-representative of actual scenario is not adequately considered. Relevant temperature variation, high humidity level, significant vibration stresses, mechanical shocks are only a few lists of environmental factors that profoundly affect the performances of microelectronic devices [27]-[30].

For this reason, this paper deals with the characterization of a commercial MEMS-based IMU stimulated with vibration stress well-representative of the actual automotive environment. A previous work published on [32] highlighted the analog antialiasing filter's inadequate performances embedded in the IMU under test. Thus, this research aims to analyze the IMU frequency response under test in the presence of an additive high-frequency white gaussian noise, typical of

the automotive context. To do that, a suitable test plan and testbed have been designed and developed to carry out the IMU characterization through a vibration shaker. The developed vibration profile is based on a mixed test including a low-frequency sinusoidal stimulus and a wideband random vibration.

Unfortunately, no international testing standards related to the test of IMUs are available, and a specific procedure for MEMS devices is missing. Consequently, international standards regarding the environmental test of electronic devices for the automotive application have been used to customize the proposed test plan.

The vibration tests have been carried out at the Analytical group test laboratory located in Scandicci, Florence (Italy).
The rest of the paper is organized as follows: Section II illustrates the preliminary work presented in a previous paper; in section III, the proposed test plan is described along with the automatic measurement system developed for this work; section IV reports the experimental results achieved with the proposed test plan.

II. Preliminary Work

A preliminary work published in [31] introduces an innovative vibration step-stress test to investigate a widely-used MEMS-based IMU frequency response in case of vibration stress at different frequencies. In particular, the Devices Under Test (DUTs) are a set of three MEMS-based Inertial Measurement Units, each one integrating two MEMS sensors:

- A triaxial accelerometer characterized by a linear acceleration full scale of ±2g/±4g/±8g/±16g , sensitivity of 0.732 mg/LSB in case the highest full scale is selected, and a linear acceleration typical zero-g level offset accuracy at full scale of ±90 mg.
- A triaxial gyroscope characterized by an angular rate full scale of ±245/±500/±2000 dps which can achieve a sensitivity of 70 mdps/LSB when it operates at ±2000 dps full scale and an angular rate typical zero-rate level at full scale of ±30 mdps.

The IMUs have been connected to three Nucleo-64 developing boards by "STMicroelectronics" based on an STM32F401RE microcontroller [33] to acquire data transfer them to a PC for storage purpose using a serial interface. The output data rate (ODR) of each sensor has been set equal to 119 Hz since it is a classical choice for many positioning algorithms.

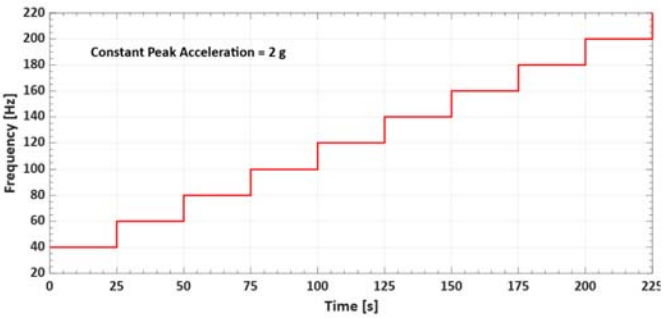

Fig. 1. Extract of the vibration step-test profile in the frequency range 40-200 Hz. Source [31]

Table I. Severity of the vibration step-test proposed in [31]

Parameter	Test level
Minimum frequency	40 Hz
Maximum frequency	2 kHz
Frequency step	+20 Hz
Vibration stress	2 g peak acceleration
Type of vibration	Sinusoidal
Holding time at each step	25 s
Number of cycles	1
Axis	X, Y, and Z

In this case, an analog antialiasing filter of 50 Hz is automatically introduced on each axis and each sensor.

The IMUs under test have been subjected to a sinusoidal vibration at different frequencies, maintaining a constant peak acceleration. The development of the test plan is based on the widely known sine sweep vibration profile defined and illustrated in many international standards, such as the European standard IEC 60068-2-6 (2009) [34] and the military standard MIL-STD-810G (2008) [35] regarding the environmental engineering considerations and laboratory tests of electronic equipment. The test plan developed in [32] is a sort of vibration step-test, where the physical quantity that steps up is not the peak acceleration but is the frequency of the stimulus. More in detail, the test involves a single frequency sweep focused on a single freezed frequency for a fixed period of holding time. After such a period of time, the frequency will be subjected to a fixed step-up. The severity of the test is illustrated in table 1, while Fig.1 shows an extract of the test profile (i.e., only the subrange 40 – 200 Hz is considered in the figure).

The discussion of the experimental results presented in [31] highlights many interesting findings. First of all, all the accelerometer's axes not interested directly by the excitation shown an unexpected behavior (regardless of the axis on which the stimulus is applied). More in detail, their outputs are significantly different from zero, leading to the presence of an undesired cross-axis sensitivity. Moreover, despite a low-pass filter at 50 Hz, the sensors' outputs follow the expectation only up to 400 Hz. After that, the outputs of all the axis start present suddenly gains and not linear response. All the sensors' axes measure high acceleration levels at a frequency higher than 1 kHz, which was not expected since the test plan involved a constant peak acceleration over the whole frequency range. The worst behavior was exhibited by applying stimulus on the z-axes, where both cross-sensitivity and unexpected high-frequency gain reached extremely high levels. The same results have been obtained for all the DUTs under test, both for accelerometer and gyroscopes, confirming the presence of an important deviation of the operation from the expected one. For example, the Root Mean Square value of the accelerometer's output is illustrated in Fig. 2, considering the vibration stress applied on the y-axis.

III. Proposed Test Plan

This work proceeds the characterization presented in [31], illustrating a new vibration-based test plan's experimental results. The DUTs and the measurement setup are the same ones

tested on [31] to ensure significant results.
This work's testing profile aims to analyze the problems raised in [31] through the so-called Sine-On-Random testing procedure. The current test plan has been customized on the actual automotive scenario using an electronic device's real operating stimuli for automotive application. According to the international standard ISO 16750-3:2003 [36] (Road vehicles-Environmental conditions and testing for electrical and electronic equipment – Part 3: Mechanical loads), the vibration endured by an electronic device mounted on a road vehicle can be divided into two types:

- Sinusoidal vibration: it could be one of the spectral components from the acceleration due to the vehicle's motion, or it could be caused by unbalanced mass forces, vibration induced by the pulsation of the intake air, etc.…
- Random noise from all the other vibration sources of an engine (e.g., closing of valves), the noise created by the gearwheels' friction, random vibration induced by rough-road-driving.

Consequently, ISO 16750-3:2003 [35] suggests performing the test as a combined sine and random test in compliance with International Standard IEC 60068-2-80 [37]. The latter defines "swept frequency sinusoidal vibration on wideband random vibration" or simply Sine-On-Random as one or more sinusoids swept over a frequency range and superimposed on random vibration. In other words, this kind of vibration test is based on the application of two different vibration stimuli at the same time: wideband random vibration stress and a sinusoidal vibration stimulus. This test requires the definition of a composite vibration severity, consisting of swept frequency sinusoidal components on a random background. In some instances, the sinusoidal stimulus could be maintained fixed instead of being swept over a frequency range.
Consequently, both sinusoidal and random vibration severities have been customized on the actual operating condition related to the application field.
Regarding the sinusoidal vibration, this stimulus is a low-frequency sinusoid with a vibration peak of 1 g. Both frequency and amplitude are maintained constant over the testing time. This vibration stands for a hypothetical IMU input signal, which must be acquired without distortion since it represents the acceleration that the positioning algorithms must process. The truthfulness of this vibration has been proven in a previous work [38] in which a suitable measurement system was

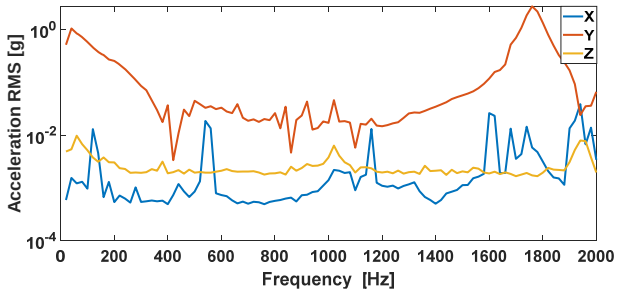

Fig. 2. RMS accelerometer's output with stimulus applied to the y-axis. Source [31].

proposed to evaluate the driver's exposure to vibration during a ride on a motorcycle. The paper highlights that the vibration analysis band for a motorcycle varies from 0.25 Hz to 20 Hz. Therefore, four different service conditions (SC) have been developed to recreate the automotive application's actual vibration. For simplicity, the service conditions are based on a single sinusoid, which is not the real vibration experienced in the automotive field. Instead, it is only a single spectral component of the actual vibration. Three SCs are based on a single sinusoid with constant frequency(i.e., 5 Hz – 10 Hz – 15 Hz), while the last one is based on a frequency sweep from 5 Hz to 20 Hz.
The wideband random vibration is based on the excitation of all the frequencies in a defined spectrum at any given time. This test is extremely useful since vibrations found in everyday life scenarios are not repetitive or predictable like sinusoidal waveforms. The severity of random vibration is described as providing an Acceleration Spectral Density (ASD) over a frequency range. The proposed test plan is based on a constant $ASD = 0.01\ g^2/Hz$ over the frequency range from 200 Hz to 2 kHz. This represents a wideband gaussian white noise that could distort the low-frequency signal related to the monitored item's actual motion. Because of the ODR of the DUTs, a 50 Hz antialiasing filter is introduced on the IMU (see section II). Consequently, the random vibration should be completely cut-off by the antialiasing filter. Instead, as extensively explained in [32], the accelerometer's output shows an unexpected high-frequency gain.

Several standards agree that the vibration endured by an electronic device for automotive application is a wideband stimulus with a maximum frequency of up to 2 kHz. The frequency range is strictly related to the exact deployment of the DUT. The most significant standards taken into account during the development of the proposed test plan are the following:

- ISO 16750-3 was released in 2003 by International Organization for Standardizations [36]. It describes the mechanical loads that can affect electronic equipment mounted on-road vehicles.
- IEC 60068-2-64 released on 2008 by International Electrotechnical Commission [39]. It is a general standard that regulates random vibration testing.
- ETSI EN 300 019-2-5 was released in 2002 by the European Telecommunications Standards Institute (ETSI) [40]. It deals with environmental testing for telecommunications devices installed in ground vehicles.
- AEC-Q100-rev.H was released in 2014 by the Automotive Electronics Council [41]. It provides a set of qualification tests for integrated circuits used on automotive applications.

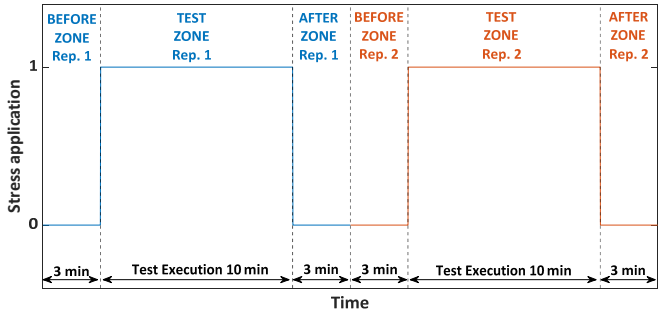

Fig. 3. The test procedure's schematic representation is divided into three zones: before zone, test zone, and after zone. The different colors stand for different repetitions of the same service condition.

Table II summarizes the normative references used to identify the frequency range of the random vibration concerning installation type.

Most of the standards agree that devices mounted on-road vehicles are subjected to random vibration up to 2 kHz. This is why the proposed test plan includes a random vibration over the frequency range from 200 Hz to 2 kHz, although the ODR of the sensor is 119 Hz.

Table III summarizes the severity of the proposed test plan highlighting the four different SCs. Note that the random vibration is kept unchanged for all service conditions.

Additional information regarding the test are illustrated in the following:

- Test duration: 10 minutes.
- Axes involved: X, Y, and Z.
- Repetition: 5 consecutive tests for each SC of each axis.

Table II. Normative reference for random vibration testing: equipment installed on a ground vehicle

Type of installation	Maximum frequency	Reference standard
Equipment mounted directly on the engine	up to 2 kHz	ISO 16750-3
Gearbox mounted equipment	up to 2 kHz	ISO 16750-3
Equipment mounted on sprung masses (vehicle body)	up to 1 kHz	ISO 16750-3
Equipment mounted on unsprung masses (wheel, wheel suspension)	up to 2 kHz	ISO 16750-3
Automotive application: Integrity test for semiconductor devised	Up to 2 kHz	AEC-Q100
Automobile, chassis-mounted.	up to 1 kHz	IEC 60068-2-64
Automobile, engine compartment, attached to the body or on the radiator.	up to 0.2 kHz	IEC 60068-2-64
Telecommunication equipment mounted on a ground vehicle	up to 0.5 kHz	ETSI EN 300 019-2-5

Table III. Summary of the developed test plan: four service conditions with different severities have been proposed.

Service condition	**Sinusoidal Vibration**		**Random Vibration**	
	Frequency	**Peak vibration**	**Frequency range**	**ASD [g^2 / Hz]**
SC 1	5 Hz	1 g	200 – 2000 Hz	0.01
SC 2	10 Hz	1 g	200 – 2000 Hz	0.01
SC 3	15 Hz	1 g	200 – 2000 Hz	0.01
SC 4	Sweep from 5 Hz to 20 Hz Sweep rate 1 oct/min	1 g	200 – 2000 Hz	0.01

- The same fixture must be used for all the test run along the same axes.
- For the sake of repeatability, several test repetitions must be carried out without dismounting and remounting the DUTs to the vibration table (so the position stays the same) to minimize the mounting uncertainties. This is fundamental to ensure that any mechanical load due to the fixture of the DUTs to the shaker remains the same in all the repeated tests.

Each test repetition is based on three different phases:

- "Before zone": 3 minutes of acquisition before the application of the vibration profile. No stress is involved.
- "Test zone": data acquisition during the test (10 minutes).
- "After zone": 3 minutes of acquisition after the application of the vibration profile. No stress is involved.

This kind of acquisition allows comparing the performances of the DUTs before and after the stress application to identify potential failure mechanisms or any possible damages that the test could trigger. Fig. 3 summarizes this concept illustrating with different colors two consecutive repetitions of the same service condition.

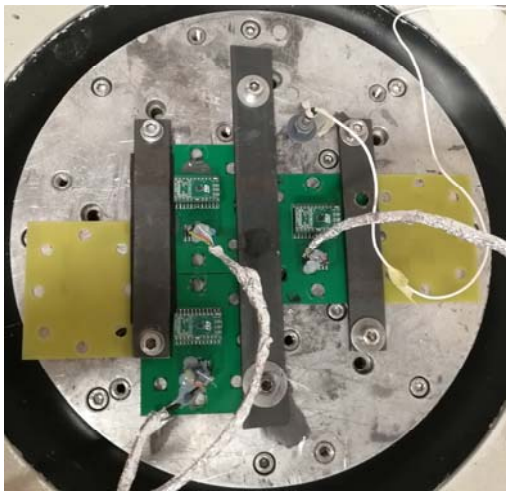

Fig. 4. Picture of the three DUTs mounted on the vibration generator during the test (Z-axis is involved).

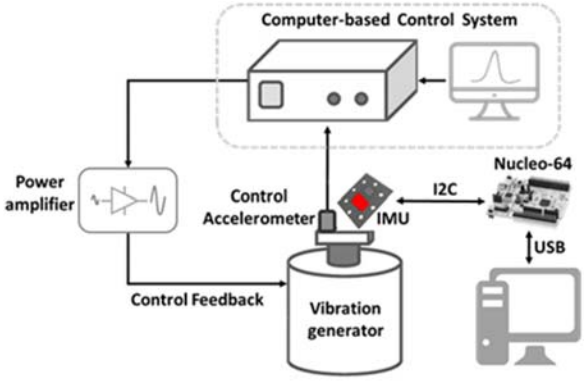

Fig. 5. Complete testbed developed for this project, including the vibration testing system, the device under test, and the acquisition system.

To ensure repeatability of the results, every test repetitions of each SC of the same axes have been performed using the same fixture, without dismounting the setup between one acquisition and the following one. An example of a fixture used for the Z-axis is illustrated in Fig. 4.

As for the X-axis and Y-axis, they were separately excited by suitably arranging the DUTs according to the shaker reference system. In particular, as for the X-axis, all the DUTs have been oriented parallel to the direction of the vibration stress provided by the shaker, whereas, as for the Y-axis, all the DUTs have been oriented perpendicular to the direction of the vibration stress provided by the shaker.

The test method is based primarily on an electrodynamic or a servo-hydraulic vibration generator (also known as shaker) with an associated computer-based control system used as a vibration testing system. More information about the test-bed used for the characterization of the IMUs under vibration conditions are reported in [30].

For the sake of repeatability, the exact vibration provided by the shaker during the test execution is measured using a "control accelerometer". The latter is directly connected to the computer-based control system which uses a feedback to actuate the vibration shaker based on the response of the control accelerometer. Fig. 5 illustrates the complete testbed developed in this work, including both the vibration testing system and the acquisition system required to store the data monitored by the IMUs.

According to the test plan, taking the Service Condition SC 2 as an example, Fig. 6 shows the shaker's vibration profile. The signal has been monitored by the control accelerometer located on the shaker slip table (see Fig. 5).

Fig. 6 illustrates the spectral acceleration density generated by the shaker over the considered frequency range. It is visible the 10 Hz sinusoid and the wideband white noise over one order of magnitude lower than the sinusoids. It also presents an additive noise over the frequency domain not covered by the sinusoids and the random vibration (i.e., for frequencies lower than 10 Hz and frequencies from 10 Hz to 2 kHz). Despite this, the latter noise is over two orders of magnitude lower than the gaussian white noise, and thus it could be neglected.

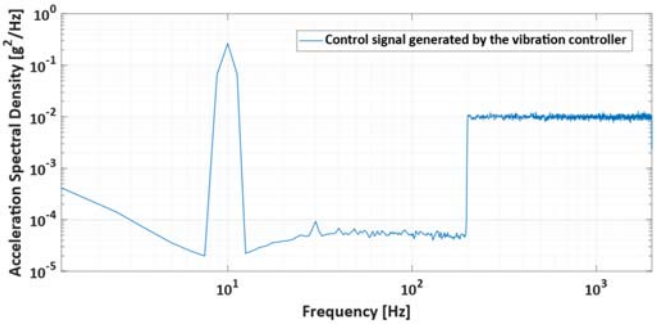

Fig. 6. Test Condition SC2: Vibration profile generated by the shaker and measured by the control accelerometer mounted on the table.

IV. Experimental Results

Below are reported the experimental results obtained during the excitation of the three DUTs presented considering the test profile described in section III. The test aims to evaluate both the potential failure mechanisms or any possible damages on the DUTs and analyze their operation during the test's execution. For this reason, the experimental results section has been divided into two different subsections: the former reports the results of an analysis "Before-After" introduced in [30], while the latter reports the evaluation of particular indexes devoted to the exploration of the DUT's behaviors under the excitations. . Also if the DUT is factory calibrated, to eliminate residual gain and offset errors due to the final installation and soldering on development board, an initial 6-point tumble sensor calibration has been taken into account according to [31].

a) Before and After analysis

According to Fig.3, the accelerometers' output and the gyroscopes of devices under test have been acquired during quiet zones of equal length before and after applying excitations described in section III.

From one hand, this test aims to verify the impact of the proposed excitation on the DUTs. Generally, the test can report unwanted inducted miscalibration on the sensors after the test or permanent damages.

The outcome of these analyses is extremely important. Indeed, the evidence that no critical influences are exhibit after the tests reveal that the analysis during the test zones (reported in the following subsections) has significance. At the same time, the "Before-After" analysis can show how much DUTs are reliable in terms of any potential failure mechanisms or any possible damages during the entire experimental test.

For example, Table IV reports, for the three DUTs, the mean and standard deviation of acquisitions before and after the testing zone for SC 1 (see Table III). In particular, for the sake of brevity, the results related to the accelerometer sensors when the excitation is applied on the x-axis are reported.

According to Table IV, and better represented in Fig. 7, the observed full compatibility (from a measurement point of view)

among all the "before" and "after" conditions for all the repetitions and sensors considered indicates two principal aspects: i) the tests have not influenced the devices operativity, ii) non-miscalibration phenomenon (i.e., a changing of the mean value) has been observed during all the tests.

More in detail, Fig. 7 reports the error plots of the DUT#1 x-axis, extracted from Table IV. In particular, the comparison of the measurements relative to the single repetition can be easily evaluated by analyzing the blue lines (relative to the zone before the SC1 test) the red lines (relative to the zone after the SC1 test).

Similar results have been obtained considering both the excitation on the y and z axes and the other Service Conditions (SC2, SC3, and SC4).

The same approach has been considered for the gyroscope sensors, obtaining the full compatibility of measurements.

b) Test zone

The test zone has considered different indexes introduced in [30] to evaluate unwanted sensitivity phenomena on axes different from excited ones. For this reason, Rejection Ratios ($RR_{i,j}$) and Spurious response Ratios ($SR_{i,j}$) for the three axes of the sensors during the test have been evaluated according to the equation proposed in [30] and reported below:

$$RR_{i,j} = \left| 20 \cdot \log_{10} \frac{RMS_{i,TZ}}{RMS_{j,TZ}} \right| \quad (1)$$

$$SR_{i,j} = \left| 20 \cdot \log_{10} \frac{RMS_{i,TZ}}{RMS_{i,BZ}} \right| \quad (2)$$

Where i indicates the not excited (accelerometer or gyroscope) axis, j denotes the excited accelerometer axis, $RMS_{i,TZ}$ and $RMS_{j,TZ}$, the RMS values estimated in the test zone for the i and j axes, and $RMS_{i,BZ}$, the RMS value estimated in the zone before the test, for the i axis.

As a consequence, $RR_{i,j}$ describes the rejection ratio of the i axis when the excitation is applied on the j axis whereas, $SR_{i,j}$ provides the ratio between the spurious response of the DUT on the considered axis concerning the expected value (i.e., the quiet zone value).

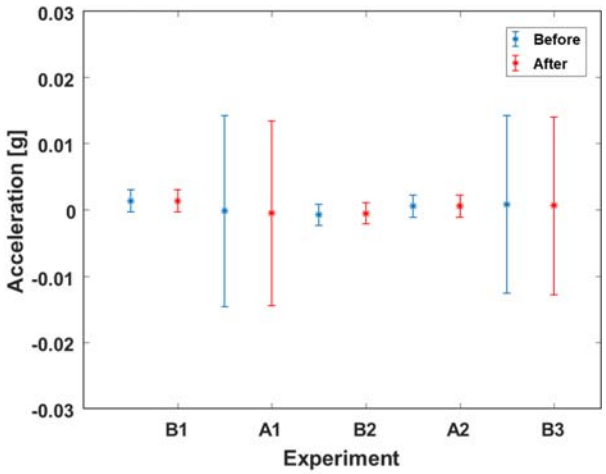

Fig. 7. Test Condition SC1: Error Bar for the analysis "Before - After" of DUT#1 when the excitation is applied on the x-axis, and the accelerometers sensors are involved.

Besides, due to the nature of the new test plan proposed, which consists of a sine vibration at a single frequency belonging to a particular scenario related to the slow movement of suspended masses in vehicles, with the addition of random vibration, the Signal to Noise Ratio (SNR) has been evaluated with and without the random vibration introduced in the SC conditions.

- ***$RR_{i,j}$ and $SR_{i,j}$***

Starting from the $RR_{i,j}$ index analysis, Table V reports these values calculated for the SC1 during the test zone.

In particular, to prove that tests results are consistent throughout the "Test Zone" five repetitions for the three DUTs

Table IV. "Before- After" analysis for the three axes of the accelerometer sensors when the excitation is applied on the x-axis.

	X-axis [g]				Y-axis [g]				Z-axis [g]			
	Before Test		After Test		Before Test		After Test		Before Test		After Test	
	mean	std	mean	std	mean	std	mean	std	mean	std	mean	std
DUT#1	0,0013	0,0017	0,0013	0,0017	-0,0003	0,0019	-0,0003	0,0019	-0,0003	0,0019	-0,0003	0,0019
	-0,0002	0,0144	-0,0005	0,0139	0,0006	0,0017	0,0003	0,0017	0,0006	0,0017	0,0003	0,0017
	-0,0008	0,0016	-0,0006	0,0016	0,0007	0,0021	0,0008	0,0020	0,0007	0,0021	0,0008	0,0020
	0,0005	0,0017	0,0005	0,0017	-0,0007	0,0019	-0,0006	0,0018	-0,0007	0,0019	-0,0006	0,0018
	0,0008	0,0134	0,0006	0,0134	0,0018	0,0017	0,0015	0,0017	0,0018	0,0017	0,0015	0,0017
DUT#2	-0,0004	0,0016	-0,0001	0,0016	0,0001	0,0020	0,0002	0,0020	0,0001	0,0020	0,0002	0,0020
	-0,0012	0,0017	-0,0012	0,0017	0,0001	0,0019	0,0001	0,0019	0,0001	0,0019	0,0001	0,0019
	-0,0004	0,0139	-0,0006	0,0124	0,0011	0,0017	0,0008	0,0017	0,0011	0,0017	0,0008	0,0017
	-0,0003	0,0017	-0,0004	0,0017	-0,0006	0,0020	-0,0006	0,0021	-0,0006	0,0020	-0,0006	0,0021
	-0,0001	0,0017	-0,0001	0,0017	0,0011	0,0019	0,0011	0,0019	0,0011	0,0019	0,0011	0,0019
DUT#3	0,0010	0,0125	0,0006	0,0125	-0,0002	0,0017	-0,0002	0,0017	-0,0002	0,0017	-0,0002	0,0017
	-0,0005	0,0017	-0,0001	0,0017	0,0002	0,0021	0,0003	0,0073	0,0002	0,0021	0,0003	0,0073
	-0,0009	0,0017	-0,0009	0,0017	-0,0001	0,0019	-0,0002	0,0019	-0,0001	0,0019	-0,0002	0,0019
	0,0004	0,0126	0,0003	0,0120	-0,0002	0,0017	-0,0003	0,0017	-0,0002	0,0017	-0,0003	0,0017
	-0,0005	0,0017	-0,0006	0,0017	-0,0002	0,0072	-0,0003	0,0021	-0,0002	0,0072	-0,0003	0,0021

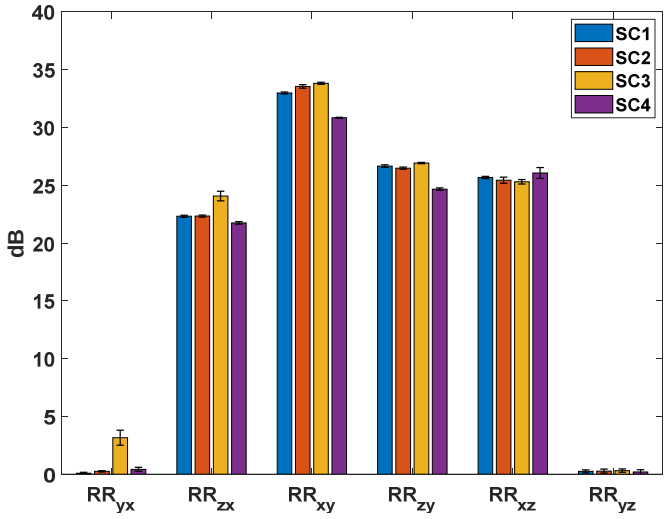

Fig. 8 Bar graph of the mean value of the $RR_{i,j}$ indexes over all the repetitions for the different SC conditions (accelerometer of DUT#1 is involved).

have been reported, and the excitation on the three different axes have been considered. Ideally, the $RR_{i,j}$ should tend to infinite, representing the ideal case where the excitation provided on an axis does not influence the non-excited axis considered for the analysis.

The analysis of Table V can draw many results:

- with except for one case (i.e., DUT#2, Rep. 2), whatever be the DUT and $RR_{i,j}$, the achieved results show good repeatability;
- all DUTs generally show a non-ideal behavior in terms of cross-sensitivity for some couples of axes. This can be imputable to their internal structure, which cannot perfectly avoid the partition of mechanical stress on a not excited axis;
- as for DUT#1, the worst performance is observed for $RR_{y,x}$ and for $RR_{y,z}$ which means that the *y*-axis is the most sensitive to vibrations applied on the other axes (*x* and *y*, respectively);
- as for DUT#2, the worst performance is observed for $RR_{y,x}$, and for $RR_{x,z}$, which means that both *the y*-axis and the *x*-axis are the most sensitive to vibrations applied on the other axes (*x* and *z*, respectively);
- as for DUT#3, the worst performance is observed for $RR_{x,z}$ and for $RR_{y,z}$, which means that the excitation on the z-axis brings to the highest cross-sensitivity concerning the other axes;
- The different behaviors among the DUTs in terms of $RR_{i,j}$ values (for a given couple of *i*,*j* they show different values of $RR_{i,j}$) and of couples of axes showing the worst performance can be due to the intrinsic features' dispersion of the considered low-cost DUTs.

Table V. Rejection ratios for the three axes of the accelerometer sensors for the SC1 test.

DUT	Rep.	RR_{yx} [dB]	RR_{zx} [dB]	RR_{xy} [dB]	RR_{zy} [dB]	RR_{xz} [dB]	RR_{yz} [dB]
DUT #1	Rep.1	0,2	22,3	32,9	26,6	25,6	0,2
	Rep.2	0,0	22,4	32,9	26,6	25,6	0,2
	Rep.3	0,1	22,2	32,9	26,6	25,7	0,2
	Rep.4	0,1	22,3	33,0	26,7	25,8	0,5
	Rep.5	0,0	22,4	33,1	26,8	25,8	0,2
DUT #2	Rep.1	2,9	27,2	22,7	55,6	6,5	52,1
	Rep.2	3,0	27,3	22,3	46,1	8,7	22,4
	Rep.3	3,2	27,3	22,1	55,5	7,1	49,5
	Rep.4	3,0	27,3	22,0	57,5	5,2	49,3
	Rep.5	3,1	27,3	21,9	57,8	4,8	52,8
DUT #3	Rep.1	7,6	23,5	33,4	32,7	2,6	0,5
	Rep.2	7,3	23,5	33,8	32,8	2,7	0,5
	Rep.3	6,8	23,4	33,9	32,9	2,8	0,4
	Rep.4	6,9	23,5	33,5	32,9	2,9	0,3
	Rep.5	6,6	23,4	34,1	32,8	2,9	0,4

The results reported in Table V consider only the SC1 test for accelerometers, but similar behaviors can be drawn for the SC2, SC3, and SC4 tests and gyroscope sensors. Comparing the behaviors obtained for different SC, it reveals a weak influence of the particular SC main frequency on $RR_{i,j}$, as also proved by Fig. 8-9. More in detail, these figures report the mean values of the $RR_{i,j}$ together with the corresponding standard deviations calculated over the five repetitions for DUT#1, and for each SC considering respectively accelerometer in Fig. 8 and gyroscope in Fig. 9.

Similar results have been achieved in the case of DUT #2 and DUT #3.

As for the analysis of the $SR_{i,j}$, such a figure of merit poses the focus on the spurious rejection ratio among the measures regarding the quiet zone before each SC test zones and SC test zones for the non-excited axes. This index should be ideally zero, representing the scenario in which applying the excitation on a particular axis *j*, it does not influence the ratio among the measured RMS value of a non-excited axis *i*, evaluated before and during the stimulus's application.

Table VI reports the $SR_{i,j}$ indexes for the SC1 condition for the three DUTs and five repetitions. Looking at the results achieved, some considerations can be drawn:

- the first and the last column of Table VI, representing the evaluation of the spurious rejection analysis for the *y*-axis when excitation is applied on the *x*-axis and the *z*-axis, respectively, reveals to be the worst case. Therefore, once again, the lower rejection ability of the *y*-axis seems to be confirmed;
- with except for some cases (i.e., DUT#2-Rep.2 and DUT3#-Rep.1, and DUT#3-Rep.5), whatever be the DUT, the achieved results show good repeatability;
- Again, the differences among the DUTs in terms of $SR_{i,j}$ can be imputable to the intrinsic features' dispersion of the considered low-cost DUTs.

Similar results have been obtained for the other SCs in the case of the accelerometer sensors, as showed in Fig. 10. In such a case, the similar behaviours obtained among the different SCs

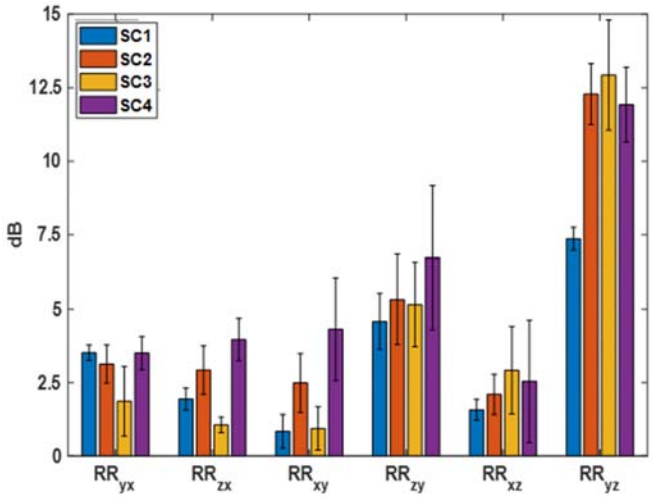

Fig. 9 Bar graph of the mean value of the RRi,j indexes over all the repetitions for the different SC conditions (gyroscope of DUT#1 is involved)

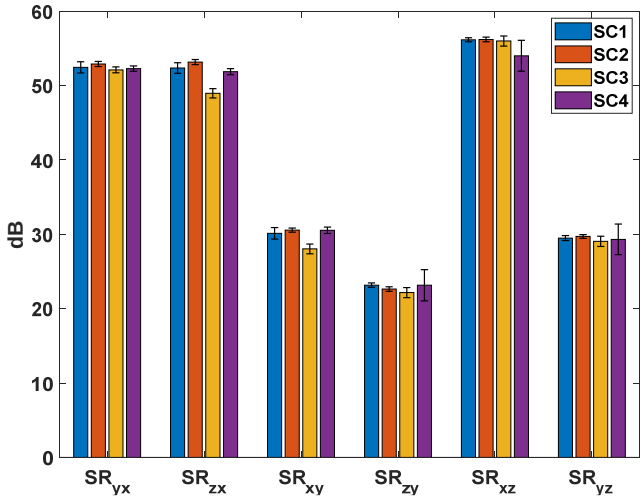

Fig. 10 Bar graph of the mean value of the $SR_{i,j}$ indexes over all the repetitions for the different SC conditions (accelerometer of DUT#1 is involved).

reveal a low influence of the particular SC's main frequency on $SR_{i,j}$.

As for the gyroscope sensors, Fig. 11 shows how the behavior is less regular concerning the accelerometer sensors. Indeed, in the case of $SR_{y,x}$ and $SR_{z,x}$, such values are weakly influenced by the considered SC (i.e., main frequency of the vibration), whereas in the other cases ($SR_{x,y}$, $SR_{z,y}$, $SR_{x,z}$ and $SR_{y,z}$) either SC3 or SC4 show higher values.

These results can be imputable to the gyroscope's intrinsic features: indeed, typically, they are devoted to measure only the rotational rate; however, in a real scenario, gyroscopes exhibit sensitivity to acceleration mostly due to the asymmetry of their micromachining inaccuracies and mechanical designs. These facts lead to significant sensitivity to linear acceleration and vibration rectification, representing the largest error source. More importantly, low-cost gyroscopes are often not optimized for vibration rejection since they are generally designed using compact and straightforward mechanical systems. In addition gyroscopes are prone to drift, representing an additional error source. This phenomenon is mainly due to two causes: a slow-changing, named bias instability and a higher frequency noise variable reported in scientific literature as Angular Random Walk (ARW) [42].

Table VI. Spurious Rejection ratios for the three axes of the accelerometer sensors for the SC1 test.

DUT	Rep.	$SR_{y,x}$ [dB]	$SR_{z,x}$ [dB]	$SR_{x,y}$ [dB]	$SR_{z,y}$ [dB]	$SR_{x,z}$ [dB]	$SR_{y,z}$ [dB]
DUT #1	Rep.1	52,8	30,7	23,4	29,8	27,7	53,1
	Rep.2	52,5	30,1	23,2	29,5	27,4	52,8
	Rep.3	52,2	30,1	23,0	29,3	26,6	52,1
	Rep.4	53,0	30,9	23,4	29,8	28,5	53,2
	Rep.5	51,2	28,9	22,8	29,0	25,9	51,4
DUT #2	Rep.1	50,0	25,7	35,7	37,5	42,7	43,2
	Rep.2	49,9	25,6	36,1	37,5	40,9	41,6
	Rep.3	48,6	24,4	36,1	37,2	34,1	45,4
	Rep.4	49,6	25,4	34,9	35,6	36,8	48,4
	Rep.5	49,7	25,5	36,8	37,3	36,8	48,5
DUT #3	Rep.1	45,4	29,4	23,5	24,1	37,9	40,0
	Rep.2	45,5	29,3	22,9	23,9	38,6	50,8
	Rep.3	45,8	29,2	23,0	24,0	38,8	51,1
	Rep.4	46,3	29,7	23,8	24,4	38,5	51,1
	Rep.5	46,5	29,7	22,9	24,2	39,7	42,3

- ***SNR***

This test aims to compare the Signal to Noise Ratio (SNR) indexes calculated during the SC test zones and the one calculated considering only the single sine vibration (without the addition of the random noise vibration in the range 200 Hz

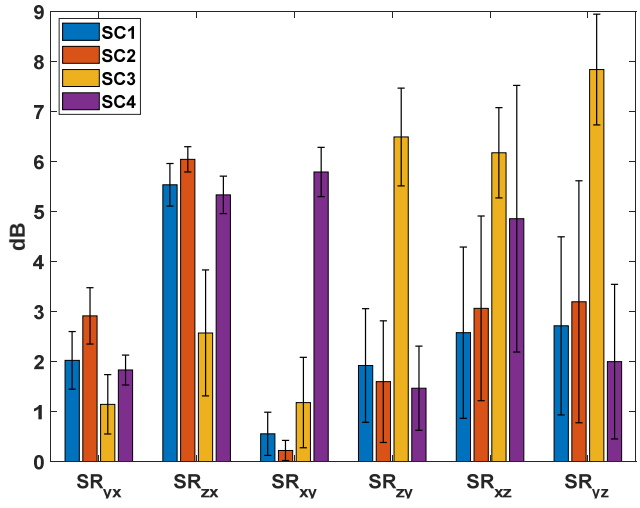

Fig. 11 Bar graph of the mean value of the $SR_{i,j}$ indexes over all the repetitions for the different SC conditions (gyroscope of DUT#1 is involved).

– 2000 Hz).

According to the Nyquist criterium, the DUT under test, selecting an output data rate (ODR) of 119 Hz, applies a low pass filter with a cut-off frequency of 50 Hz for both the gyroscope and accelerometer. The introduction of the low poss filter with the reported specification is fundamental to avoid the aliasing phenomena.

Consequently, this filter should eliminate the noise above the Nyquist frequency, mixed down into the baseband, and improving the SNR.

To evaluate the SNR on each acquisition, a MATLAB built-in function (snr) available in the Signal Processing Toolbox has been employed. This function is able to calculate the signal's spectrum and automatically labels its main features as the fundamental component, the DC value, the harmonics, and the noise.

The SNR analysis leads to evaluate its variation with and without random noise on a defined sine vibration (the main component of SC1, SC2, and SC3 condition, respectively 5 Hz, 10 Hz, and 15 Hz). These indications can qualify the sensors' ability to reject the vibration noise above the Nyquist frequency that, due to the nature of the DUTs (internal LPF with a cut-off frequency of 50 Hz in the proposed setup), should be irrelevant. To be valid, this analysis must be done on accelerometers' signal acquired on the same axes of the excitations.

Table VII reports the achieved results by comparing the reference SNR (achieved when no random vibration is applied) against the SNR achieved in the case of random vibration superimposed to the sinusoidal one in the case of SC 1 and all DUTs.

Table VII. Reference SNR (SC1 condition without random vibrations) and SNR for the three axes of the accelerometer sensors for the SC1 condition.

DUT	Rep.	SNR_x [dB]	Reference SNR_x [dB]	SNR_y [dB]	Reference SNR_y [dB]	SNR_z [dB]	Reference SNR_z [dB]
DUT #1	Rep.1	13,3	27,8	7,1	30,1	12,0	28,5
	Rep.2	13,6		7,3		12,3	
	Rep.3	13,4		7,1		11,7	
	Rep.4	13,7		7,2		12,1	
	Rep.5	13,3		7,1		11,7	
DUT #2	Rep.1	10,8	27,3	2,3	28,5	11,8	26,2
	Rep.2	10,8		2,4		12,3	
	Rep.3	11,0		2,6		12,2	
	Rep.4	11,1		2,5		12,3	
	Rep.5	11,0		2,4		11,8	
DUT #3	Rep.1	9,2	26,2	5,2	25,7	9,4	27,3
	Rep.2	9,9		5,1		9,8	
	Rep.3	9,9		5,1		9,8	
	Rep.4	10,1		5,0		9,8	
	Rep.5	10,2		5,0		9,9	

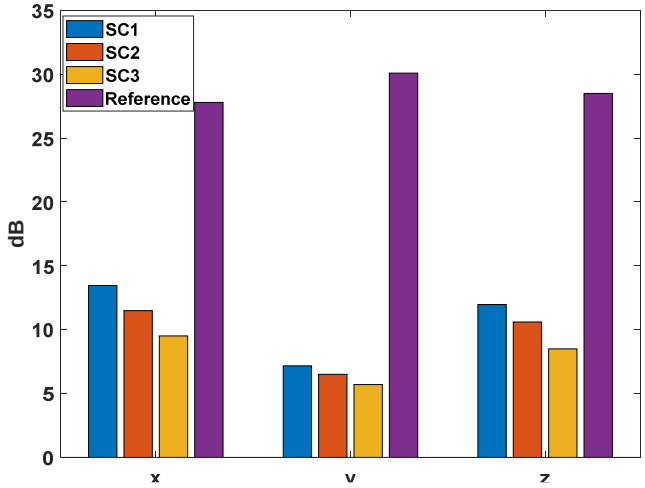

Fig. 12 Bar graph of the mean value of the *SNR* over all the repetitions for the different SC1, SC2, SC3 conditions and reference (accelerometer of DUT#1 is involved).

c) Discussion of the experimental results

Looking at results obtained from the previous subsections, the following considerations can be drawn:

- Since the SNRs values significantly decrease concerning the reference ones, it proves how the real behaviour of the antialiasing LPF filter allows be sensitive to unexpected contributions at low-frequency even if the random vibrations have been generated in the frequency range 200 Hz-2000 Hz (which is higher than the filter cut-off frequency);
- the SNR calculation over all the DUTs considering the different repetitions and the excited axis, respectively, show good repeatability (over the 5 repetitions) whatever be the DUT and the axis considered;
- according to the behaviours revealed with $RR_{i,j}$, and $SR_{i,j}$ also, in this case, the SNR indexes calculated for the *y*-axis during its excitation is smaller concerning the other ones, representing the lowest immunity (i.e., the higher sensitivity) to the random noise.

Similar behaviours have been achieved in the case of SC2 and SC3, as shown in Fig. 12, where the mean values of the five repetitions of the SNR have been reported for all the SCs with respect to the reference SNR, in the case of DUT#1. In particular, whatever be the SC, an SNR decreasing (concerning the reference one) is clearly observable.

Finally, similar behaviours have been achieved for DUT#2 and DUT#3.

V. Conclusions

In this paper, starting from standard procedures and test plans coming from international normative framework, we have proposed a new test plan for IMU devices commonly employed in terrestrial vehicles. Moreover, the paper proposes some figures of merit which allows analysing several indexes related to the performance of low-cost commercial IMUs. The main goal is to highlight the cross-axes sensitivity of the gyroscope

and accelerometer included in inertial platforms. Thus, the evaluation of Rejection Ratio ($RR_{i,j}$) and Spurious Rejection Ratio (SRi,j) have been introduced, revealing significant non-ideality of the sensors.

Moreover, the Signal to Noise Ratio (SNR) analysis among the different working conditions revealed the non-ideality of the antialiasing LPF filters in such a low-cost device. Therefore, its non-ideality can mine the reliability of measurements made by these kinds of platforms.

Besides the definition of an original test plan and a testing procedure, the achieved results are useful also for suggesting to take into account such non-idealities, thus pushing in design suitable data processing and digital filtering techniques, to be applied in real applications, to improve the measurement data's overall reliability, which in turn, could generally feed further algorithms like positioning ones.

.

REFERENCES

[1] M. Blanke, M. Kinnaert, J. Lunze, and M. Staroswiecki, *Diagnosis and Fault-Tolerant Control*. Berlin, Heidelberg: Springer Berlin Heidelberg, 2016.

[2] G. D'Emilia, A. Gaspari, E. Hohwieler, A. Laghmouchi, and E. Uhlmann, "Improvement of Defect Detectability in Machine Tools Using Sensor-based Condition Monitoring Applications," *Procedia CIRP*, vol. 67, pp. 325–331, 2018.

[3] D. Galar Pascual, *Artificial intelligence tools. Decision support systems in condition monitoring and diagnosis*. CRC Press: Taylor & Francis Group, 2015.

[4] A. González and D. Galar, "Condition monitoring of wind turbine pitch controller: A maintenance approach," in *15th IMEKO TC10 Workshop on Technical Diagnostics: Technical Diagnostics in Cyber-Physical Era*, 2017, pp. 200–206.

[5] A. Jablonski, Z. Dworakowski, K. Dziedziech, and F. Chaari, "Vibration-based diagnostics of epicyclic gearboxes – From classical to soft-computing methods," *Measurement*, vol. 147, p. 106811, Dec. 2019.

[6] G. D'Emilia and A. Gaspari, "Data Validation Techniques for Measurements Systems Operating in a Industry 4.0 Scenario a Condition Monitoring Application," in *2018 Workshop on Metrology for Industry 4.0 and IoT*, 2018, pp. 112–116.

[7] P. Qian, X. Ma, D. Zhang, and J. Wang, "Data-driven condition monitoring approaches to improving power output of wind turbines," *IEEE Trans. Ind. Electron.*, vol. 66, no. 8, pp. 1–1, 2018.

[8] L. Ciani, A. Bartolini, G. Guidi, and G. Patrizi, "A hybrid tree sensor network for a condition monitoring system to optimise maintenance policy," *ACTA IMEKO*, vol. 9, no. 1, pp. 3–9, 2020.

[9] G. D'Emilia, A. Gaspari, and E. Natale, "Amplitude–phase calibration of tri-axial accelerometers in the low-frequency range by a LDV," *J. Sensors Sens. Syst.*, vol. 8, no. 1, pp. 223–231, May 2019.

[10] D. Galar Pascual, P. Daponte, and U. Kumar, *Handbook of Industry 4.0 and SMART Systems*. CRC Press: Taylor & Francis Group, 2020.

[11] G. D'Emilia, A. Gaspari, and E. Natale, "Measurements for Smart Manufacturing in an Industry 4.0 Scenario A Case-Study on A Mechatronic System," in *2018 Workshop on Metrology for Industry 4.0 and IoT*, 2018, pp. 1–5.

[12] D. Capriglione *et al.*, "Experimental analysis of IMU under vibration," in *16th IMEKO TC10 Conference 2019 - Testing, Diagnostics and Inspection as a Comprehensive Value Chain for Quality and Safety*, 2019.

[13] G. Dissanayake, S. Sukkarieh, E. Nebot, and H. Durrant-Whyte, "The aiding of a low-cost strapdown inertial measurement unit using vehicle model constraints for land vehicle applications," *IEEE Trans. Robot. Autom.*, vol. 17, no. 5, pp. 731–747, 2001.

[14] D. Capriglione *et al.*, "Characterization of Inertial Measurement Units under Environmental Stress Screening," in *2020 IEEE International Instrumentation and Measurement Technology Conference (I2MTC)*, 2020, pp. 1–6.

[15] D. Zhao *et al.*, "Seamless integration of polarization compass and inertial navigation data with a self-learning multi-rate residual correction algorithm," *Measurement*, vol. 170, p. 108694, Jan. 2021.

[16] Y. Kamer and S. Ikizoglu, "Effective accelerometer test beds for output enhancement of an inertial navigation system," *Measurement*, vol. 46, no. 5, pp. 1641–1649, Jun. 2013.

[17] J. Botero-Valencia, D. Marquez-Viloria, L. Castano-Londono, and L. Morantes-Guzmán, "A low-cost platform based on a robotic arm for parameters estimation of Inertial Measurement Units," *Measurement*, vol. 110, pp. 257–262, Nov. 2017.

[18] J. Otegui, A. Bahillo, I. Lopetegi, and L. E. Diez, "Evaluation of Experimental GNSS and 10-DOF MEMS IMU Measurements for Train Positioning," *IEEE Trans. Instrum. Meas.*, vol. 68, no. 1, pp. 269–279, Jan. 2019.

[19] B. Alandry, L. Latorre, F. Mailly, and P. Nouet, "A CMOS-MEMS Inertial Measurement Unit," in *2010 IEEE Sensors*, 2010, pp. 1033–1036.

[20] S. C. Shen, C. J. Chen, and H. J. Huang, "A new calibration method for MEMS inertial sensor module," in *2010 11th IEEE International Workshop on Advanced Motion Control (AMC)*, 2010, pp. 106–111.

[21] Q. Chen, X. Niu, J. Kuang, and J. Liu, "IMU Mounting Angle Calibration for Pipeline Surveying Apparatus," *IEEE Trans. Instrum. Meas.*, vol. 69, no. 4, pp. 1765–1774, Apr. 2020.

[22] G. A. Aydemir and A. Saranlı, "Characterization and calibration of MEMS inertial sensors for state and parameter estimation applications," *Measurement*, vol. 45, no. 5, pp. 1210–1225, Jun. 2012.

[23] G. E. Kang and M. M. Gross, "Concurrent validation of magnetic and inertial measurement units in estimating upper body posture during gait," *Measurement*, vol. 82, pp. 240–245, Mar. 2016.

[24] S. O. H. Madgwick, A. J. L. Harrison, and R. Vaidyanathan, "Estimation of IMU and MARG orientation using a gradient descent algorithm," in *2011 IEEE International Conference on Rehabilitation Robotics*, 2011, pp. 1–7.

[25] Q. He, C. Zeng, X. He, X. Xu, and Z. Lin, "Calibrating accelerometers for space-stable inertial navigation systems at system level," *Measurement*, vol. 127, pp. 472–480, Oct. 2018.

[26] B. B. Kocer, V. E. Omurlu, E. Akdogan, and C. S. Tufekci, "Development of a MEMs-based IMU Unit," in *2013 6th International Conference on Recent Advances in Space Technologies (RAST)*, 2013, pp. 389–393.

[27] L. Ciani, D. Galar, and G. Patrizi, "Improving context awareness reliability estimation for a wind turbine using an RBD model," in *2019 IEEE International Instrumentation and Measurement Technology Conference (I2MTC)*, 2019, pp. 1–6.

[28] D. Galar, "Context driven maintenance: an eMaintenance approach," *Manag. Syst. Prod. Eng.*, vol. 3, no. 15, pp. 112–120, 2014.

[29] H. Skima, K. Medjaher, C. Varnier, E. Dedu, and J. Bourgeois, "A hybrid prognostics approach for MEMS: From real measurements to remaining useful life estimation," *Microelectron. Reliab.*, vol. 65, pp. 79–88, Oct. 2016.

[30] D. Capriglione *et al.*, "Development of a test plan and a testbed for performance analysis of MEMS-based IMUs under vibration conditions," *Measurement*, vol. 158, p. 107734, Jul. 2020.

[31] STMicroelectronics, "6-point tumble sensor calibration" https://www.st.com/content/ccc/resource/technical/document/design_tip/group0/28/fa/7d/ed/6a/41/4f/c1/DM00253745/files/DM00253745.pdf/jcr:content/translations/en.DM00253745.pdf, available online September 2021.

[32] D. Capriglione *et al.*, "Vibration Step Test for Performance Analysis of Inertial Measurement Unit," in *17th IMEKO TC 10 and EUROLAB Virtual Conference "Global Trends in Testing, Diagnostics & Inspection for 2030,"* 2020.

[33] STMicroelectronics, "STM32 Nucleo-64 boards user manual." Revision 13, 2019.

[34] IEC 60068-2-6, "Environmental testing - Part 2-6: Tests - Test Fc: Vibration (sinusoidal)." International Electrotechnical Commission, 2009.

[35] MIL-STD-810G, "Environmental Engineering Considerations and Laboratory Tests," no. October. US Department of Defense, Washington DC, 2008.

[36] ISO 16750-3, "Road vehicles - Environmental conditions and testing for electrical and electronic equipment - Part 3: Mechanical loads." International Organization for Standardization, 2003.

[37] IEC 60068-2-80, "Environmental testing Part 2-80: Tests - Test Fi:

Vibration-Mixed mode." International Electrotechnical Commission, 2005.
[38] M. Carratù, A. Pietrosanto, P. Sommella, and V. Paciello, "Smart wearable devices for human exposure vibration measurements on two-wheel vehicles," *ACTA IMEKO*, vol. 9, no. 4, p. 121, Dec. 2020.
[39] IEC 60068-2-64, "Environmental testing - Part 2: Tests - Test Fh: Vibration, broadband random and guidance." International Electrotechnical Commission, 2008.
[40] European Telecommunications Standards Institute, "Environmental Engineering (EE); Environmental conditions and environmental tests for telecommunications equipment; Part 2-5: Specification of environmental tests; Ground vehicle installations." ETSI EN 300 019-2-5, 2002.
[41] Automotive Electronics Council, "Failure Mechanism Based Stress Test Qualification for Integrated Circuit." AEC - Q100 - Rev-H, 2014.
[42] AnalogDialoge, “The Case of the Misguided Gyro”, https://www.analog.com/media/en/analog-dialogue/raqs/raq-issue-139.pdf, available online September 2021.